Acta Oceanol. Sin., 2019, Vol. 38, No. 11, P. 140–148
https://doi.org/10.1007/s13131-019-1504-5
http://www.hyxb.org.cn
E-mail: hyxbe@263.net

An accelerated nonlocal means algorithm for synthetic aperture radar ocean image despeckling

Guozhen Zha[1]*, Dewei Xu[1], Yanming Yang[1], Xin'gai Song[2], Fuhuang Zhong[1]
[1] Third Institute of Oceanography, Ministry of Natural Resources, Xiamen 361005, China
[2] National Satellite Ocean Application Service, Beijing 100081, China

Received 24 June 2018; accepted 29 September 2018

Abstract
Synthetic aperture radar (SAR) images play an increasingly important role in ocean environmental monitoring and research. However, SAR images are inherently corrupted by speckle noise. SAR ocean images have some unique characteristics. The signatures of ocean phenomena in SAR images mainly exhibit as stripe or plaque shaped features. These features typically have a high degree of self-similarity or redundancy. The nonlocal means (NLM) method can measure the structural similarity between different image patches and take advantage of redundant information in images. Considering that the NLM algorithm is computationally intensive and time-consuming, an accelerated NLM algorithm for SAR ocean image despeckling is proposed in this paper. A method is used to discriminate between texture and flat pixels in SAR images. Large similarity and search windows are used on texture pixels, whereas small similarity and search windows are used on flat pixels. Furthermore, the improved NLM algorithm is accelerated by a graphic processing unit (GPU) based on the compute unified device architecture (CUDA) parallel computation framework. The computational efficiency is improved by approximately 200 times.

Key words: synthetic aperture radar, speckle noise, ocean, nonlocal means method, compute unified device architecture

Citation: Zha Guozhen, Xu Dewei, Yang Yanming, Song Xin'gai, Zhong Fuhuang. 2019. An accelerated nonlocal means algorithm for synthetic aperture radar ocean image despeckling. Acta Oceanologica Sinica, 38(11): 140–148, doi: 10.1007/s13131-019-1504-5

1 Introduction

Since the Seasat satellite was launched in 1978, scientists have unexpectedly found that synthetic aperture radar (SAR) can provide a unique perspective of the ocean surface. Spaceborne SAR can monitor a large area of the ocean surface with high spatial resolution under all sunlight and weather conditions (Yang et al., 2010; Wang et al., 2013). It can capture various dynamic oceanographic phenomena, such as surface waves, swells, fronts, eddies, internal solitary waves, upwellings and oil slicks (Johannessen et al., 1996; Liu et al., 1998; Solberg et al., 2007; Zheng et al., 2007; Li et al., 2014). Furthermore, SAR images can also be used to extract the parameters of ocean phenomena (Alpers et al., 2013; Shen et al., 2014). At the present time, spaceborne SAR images are one of the most important tools for marine environmental monitoring and research.

However, SAR images are inherently corrupted by speckle noise, which is caused by the coherent nature of sensor and signal processing. Speckle noise dramatically degrades image quality and makes target detection, classification and tracking more difficult. Speckle noise is typically modeled as multiplicative Rayleigh noise. Compared with typically additive noise, multiplicative noise is more difficult to be suppressed without blurring fine features in SAR images.

Scientists have proposed many despeckling methods during the past decades. These methods are generally classified into two categories: multilook incoherent averaging and post-image-formation filtering. Multilook averaging methods provide a suppression of speckle, but cause a reduction in spatial resolution. Therefore, post-image-formation methods were developed to overcome this disadvantage. Generally, these methods can be divided into two approaches: spatial domain filtering and transform domain filtering. Classical spatial domain despeckling techniques, such as the Lee filter (Lee, 1980), Frost filter (Frost et al., 1982), Kuan filter (Kuan et al., 1987), and Gamma maximum a posteriori filter (Lopes et al., 1990) are based on local prior statistical knowledge about speckle noise; however, they fail to preserve texture if the statistical descriptions of speckle are inaccurate. Other spatial domain filtering methods and partial differential equation-based filtering methods have also been proposed by scientists (Wu and Maitre, 1992; Walessa and Datcu, 2000; Kervrann et al., 2007; Aubert and Augol, 2008). However, these methods also exhibit limitations in heterogeneous areas. Together with the great breakthrough made by wavelet and multiscale analysis, many transform domain filtering methods have been proposed. In transform domain filtering, images are first transformed into a domain other than spatial, and then domain specific properties are exploited to process images (Argenti and Alparone, 2002; Xie et al., 2002; Achim et al., 2003; Foucher et al., 2006; Li et al., 2011). These methods achieve very good despeckling results.

Most traditional despeckling methods encounter two common shortcomings. First, only local statistical information is con-

Foundation item: The Scientific Research Foundation of Third Institute of Oceanography, SOA under contract No. 2015008; the National Natural Science Foundation of China under contract No. 61601132.
*Corresponding author, E-mail: myfirstone@126.com

sidered and the restored value of a pixel is obtained as the average of its neighboring pixels. Second, the structural patterns and textural information in an image generally are neglected. In fact, most images contain many similar structural patterns. Buades et al. (2005) proposed a distinctive denoising approach called nonlocal means (NLM), which is based on the concept that any noisy pixel located at the center of an image patch may be denoised by building relevant statistics from other patches that have similar structures and locate at anywhere in the image. The method can efficiently decrease noise while preserving fine structures (Parrilli et al., 2012; Zhong et al., 2014). Then, many improved NLM algorithms were developed (Dabov et al., 2007; Kervrann et al., 2007; Katkovnik et al., 2010; Deledalle et al., 2012).

However, the improvement in image quality comes at the expense of increasing computational complexity, which makes the standard NLM algorithm impractical for real applications. Many speed-up strategies are proposed by scientists. Wang et al. (2006) reduced the computational cost by introducing an efficient summed square image scheme and fast Fourier transform. In the method of Bilcu and Vehvilainen (2007), pixels are preclassified and the weights are computed only for similar pixels. Vignesh et al. (2010) proposed a speed-up technique based on probabilistic early termination to eliminate dissimilar blocks. Xue et al. (2013) used the cosine integral image method to reduce the computational complexity of the standard NLM algorithm. Furthermore, scientists have proposed several parallel implementations of the NLM algorithm using graphic processing units (GPUs) (Goossens et al., 2010; Márques and Pardo, 2013; Cuomo et al., 2014; Feng et al., 2016).

Ocean phenomena mainly exhibit as stripe or plaque shaped structures in SAR images. These features typically have high self-similarity. Therefore, the NLM method is an appropriate method to process SAR ocean images. The information is mainly conveyed by intensities or textures (points or edges) in SAR images in applications such as target detection, classification, and tracking. Considering that the standard NLM algorithm involves huge calculations, a speed-up strategy is proposed in this paper. A method is used to discriminate between texture and flat pixels in SAR images, and the indices of texture and flat pixels are obtained. According to the indices, different sizes of similarity and search windows are used on the texture and flat pixels, respectively. Furthermore, the developed NLM algorithm is implemented using a GPU based on the compute unified device architecture (CUDA) parallel computation framework. Experimental results demonstrate that the time performance of the developed algorithm is improved by approximately 200 times compared with a straightforward central processing unit (CPU) implementation of the standard NLM algorithm.

This paper is organized as follows. In Section 2, the NLM algorithm is introduced. In Section 3, a method to discriminate between texture and flat pixels in SAR images is described. The GPU implementation of the rapid NLM algorithm is proposed in Section 4. Experimental results, discussion, and conclusions are presented in Sections 5 and 6.

2 Nonlocal means method

Most existing despeckling methods only consider the local statistical information of pixels. However, pixels typically do not exist in isolation but constitute structural patterns with surrounding pixels. To introduce the NLM method, we first provide the definition of an image patch: An image patch consists of a pixel and its neighboring pixels. Compared with a single pixel, an image patch contains more textural information. Most natural images typically contain abundant similar textural structures. As shown in Figs 1a and b, the textural structures in Patches a_1 and a_2 are similar to those in Patches b_1 and b_2, respectively.

The NLM algorithm simply attempts to take advantage of the high degree of self-similar redundancy in any natural image. The method also attempts to suppress speckle by calculating the weighted average of pixels. The main idea of the algorithm is as follows: For any Pixel L in a noisy image, the algorithm searches the entire image, for Pixel M, if it is similar to Pixel L, then it is assigned a large weight; otherwise, it is assigned a small weight. The similarity between pixels depends on the structural similarity of the image patches in which the pixels are located. For example, as shown in Fig. 1a, the texture of image Patch b_1 is more similar to that of Patch a_1 than that of Patch c_1. Therefore, when the NLM algorithm restores Pixel L_1, the weight of Pixel M_1 is greater than the weight of Pixel N_1. The scenario in Fig. 1b is similar to that in Fig. 1a.

Next, we provide a mathematical introduction of the NLM algorithm. Consider a noisy image $u(X)$, which is defined in a bounded domain $\Omega \subset R^2$, where $X = (x_1, x_2) \in \Omega$. To measure the structural similarity between pixels, we introduce the concept of the neighborhood of a pixel. In Ω, define subset N_x as the neighborhood of Pixel X. It needs satisfy the following conditions:

(1) $X \in N_x$; and

(2) if $Y \in N_x$, then $X \in N_y$.

The neighborhood of a pixel can have different sizes and shapes in a practical application. In this paper, subset N_x is also called the similarity window of Pixel X. Let $u(N_x)$ and $u(N_y)$ be the

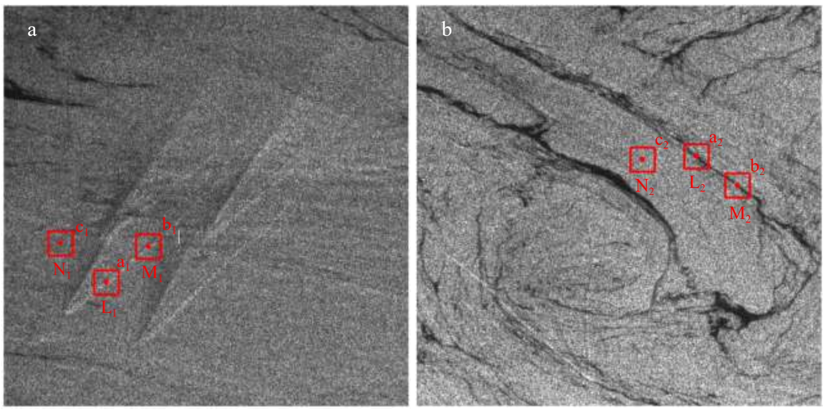

Fig. 1. Two noisy SAR ocean images. L_1, M_1, N_1, L_2, M_2 and N_2 denote the positions of six pixels in subfigures (a) and (b). a_1, b_1, c_1, a_2, b_2 and c_2 denote six image patches in subfigures (a) and (b).

image patches in which Pixels X and Y are located. They are defined as $u(N_x) := \{u(X)|X \in N_x\}$ and $u(N_y) := \{u(Y)|Y \in N_y\}$. Then, the structural similarity between Pixels X and Y is represented by the structural similarity between $u(N_x)$ and $u(N_y)$.

The structural similarity between image patches $u(N_x)$ and $u(N_y)$ is measured by the Gaussian weighted Euclidean distance:

$$(G_a * |u(X+.)-u(Y+.)|^2)(0) = \int_{R^2} G_a(T)\,|u(X+T)-u(Y+T)|^2 \mathrm{d}T, \tag{1}$$

where $T \in \Omega$ and G_a is a Gaussian kernel with standard deviation (STD) a, which is defined as

$$G_a(T) = \frac{1}{4\pi a^2}\mathrm{e}^{-|T|/(4a^2)}. \tag{2}$$

The filtered value using the NLM algorithm is computed as a weighted average of all the pixels in Ω:

$$NL(u)(X) = \frac{1}{c(X)}\int_{\Omega} \mathrm{e}^{-\frac{(G_a*|u(X+.)-u(Y+.)|^2)(0)}{h^2}} u(Y)\mathrm{d}Y, \tag{3}$$

where h is the filtering parameter that controls the decay of the exponential function and $c(X)$ is the normalized factor given as

$$c(X) = \int_{\Omega} \mathrm{e}^{-\frac{(G_a*|u(X+.)-u(Z+.)|^2)(0)}{h^2}} u(Y)\mathrm{d}Z. \tag{4}$$

For a convenient application, we consider an image defined on discrete grid I. Given discrete noisy image $u(i)$, $i \in I$, the filtered value $NL(u)(i)$ is given as

$$NL(u)(i) = \sum_{j \in I} w(i,\, j)u(j), \tag{5}$$

where weight $w(i, j)$ depends on the similarity between Pixels i and j, which is given as

$$w(i,\, j) = \frac{1}{Z(i)}\mathrm{e}^{-\frac{\left\|u(N_i)-u(N_j)\right\|^2_{2,a}}{h^2}}, \tag{6}$$

which needs to satisfy $0 < w(i, j) < 1$ and $\sum_j w(i,\, j) = 1$, $\|u(N_i)-u(N_j)\|^2_{2,\,a}$ is a Gaussian weighted Euclidean distance, and $Z(i)$ is a normalizing factor:

$$Z(i) = \sum_j \mathrm{e}^{-\frac{\left\|u(N_i)-u(N_j)\right\|^2_{2,\,a}}{h^2}}. \tag{7}$$

For computational purposes, we typically do not search the entire image but control the similarity search in a particular area called the search window. In practice, similarity and search windows are typically chosen as square windows. The NLM algorithm involves high computational complexity. For an $M \times M$ noisy image, if the sizes of the similarity and search windows are set to $d \times d$ and $s \times s$, respectively, then the computational cost of the algorithm is $O(d^2 s^2 M^2)$.

3 Discriminate between texture and flat pixels

The superior performance of the NLM method is achieved at the cost of high computational complexity, which makes the algorithm impractical for processing entire SAR images. In this section, a fast NLM computational scheme is introduced by adaptively adjusting the sizes of the similarity and search windows.

For each pixel in a noisy SAR ocean image, with the pixel as the center, a rectangular window is chosen. In this paper, the dimension of the rectangular window is chosen as 17×17. As shown by the red arrows in Fig. 2a, four mean gray values are calculated along four directions in each rectangular window. The mean gray values are denoted as $\bar{g}_k$, where k=1, 2, 3, 4 represent the four directions. Next, the sums of the absolute differences of gray values between each pixel and mean gray values $\bar{g}_k$ are calculated along four directions:

$$f_k = \frac{1}{N}\sum_{i=1}^{N} |g_{i,\,k} - \bar{g}_k|, \tag{8}$$

where $g_{i,\,k}$ is the gray value of the i th pixel in the k th direction and N=17 is the width of the rectangular window. Finally, the maximum gray value difference $f_{\max}$ is

$$f_{\max} = \max\{f_1,\, f_2,\, f_3,\, f_4\}. \tag{9}$$

If $f_{\max}$ is larger than a given threshold, the rectangular window is considered as a texture region; otherwise, it is considered as a flat region. As a result, the pixel at the center of the rectangular window is considered as a texture pixel or flat pixel. When the SAR image is processed by the NLM method, large similarity and search windows are used on texture pixels, whereas small windows are used on flat pixels.

The next question is how to determine the threshold. For a given noisy SAR ocean image, a homogenous region is selected in advance. The sum of absolute differences of gray values between each pixel and the mean gray values are calculated:

$$f = \frac{1}{N}\sum_{i=1}^{N} |g_i - \bar{g}|, \tag{10}$$

where N is the total number of pixels in the homogenous region, $\bar{g}$ is the mean gray value of the homogenous region, and g_i is the gray value of the ith pixel. In this paper, the threshold is set to $1.3f$. As shown in Fig. 2b, texture pixels are detected and painted purple for the image in Fig. 1a. Experiments demonstrate that

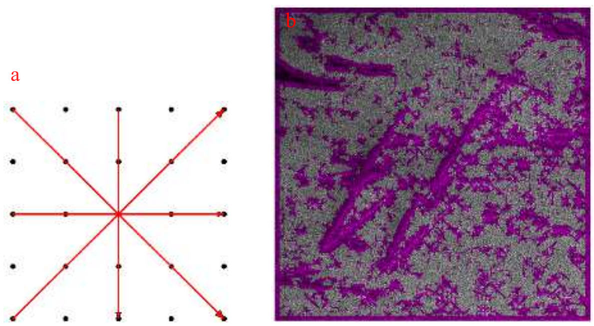

Fig. 2. The diagram of the detector and the detection result for a SAR image. a. Four directions for texture and flat pixel detection; b. texture pixels are painted purple. The dimension of the rectangular window is set to 17×17.

texture pixels can be effectively determined by the method.

4 GPU implementation of the improved NLM algorithm

CUDA was released by the NVIDIA Corporation in 2006. With the help of the new general purpose computing platform and programming model, we can use the parallel computing engine of GPUs to solve complicated computations. CUDA comes with a software environment in which the developer can use a C-like language rather than a graphic application programming interface (API) for general purpose computing.

The NLM algorithm involves a large number of calculations. However, the calculations are mainly consumed in calculating the Euclidean distances between patches and the normalizing factors. Additionally, these calculations are completely independent. Therefore, the NLM algorithm is suited to be accelerated using GPUs. The indices of texture and flat pixels can be obtained using the method introduced in Section 3. The calculations are also independent for each pixel. Large similarity and search windows are used on texture pixels, whereas small windows are used on flat pixels.

In the implementation, the serial codes are executed on the host, whereas the parallel codes are executed on the device. The procedure can be briefly described as follows: (1) a SAR image is read into host memory; (2) the SAR image is transferred to the device; (3) the coordinates of local windows are mapped to the indices of threads, the variations of gray values along four directions are calculated by different threads, and the indices of texture and flat pixels are determined; (4) the indices of image patches are mapped to the indices of threads, and the Euclidean distances between different patches and the normalizing factors are calculated by different threads; and (5) the gray values of pixels are revised by the weighted average.

The algorithm was implemented on a computer with a 3.4 GHz dual-core Intel(R) Core(TM) i7-4930K CPU, 32 GB RAM, and NVIDIA GeForce GTX TITAN Z GPU. For the proposed NLM algorithm, the similarity and search windows for texture pixels were set to 21×21 and 7×7, respectively, whereas the similarity and search windows for flat pixels were set to 13×13 and 7×7, respectively. For the standard NLM algorithm, the search and similarity windows were set to 21×21 and 7×7, respectively. The experiments demonstrated that the computational efficiency improved by approximately 200 times over a plain CPU implementation of the standard NLM algorithm.

5 Results

The despeckled results of the proposed accelerated NLM algorithm for different SAR ocean images are presented in this section. For comparison, the processed results of the standard NLM algorithm, Lee and Frost filters are also be presented.

Figure 1 shows two noisy SAR ocean images. Figures 1a and b show the signatures of ship wakes of four ships and oil films on the sea surface, respectively. Because of the inherent characteristics of fluid, the signatures of ocean phenomena in SAR images are mainly displayed as stripe or plaque shaped features.

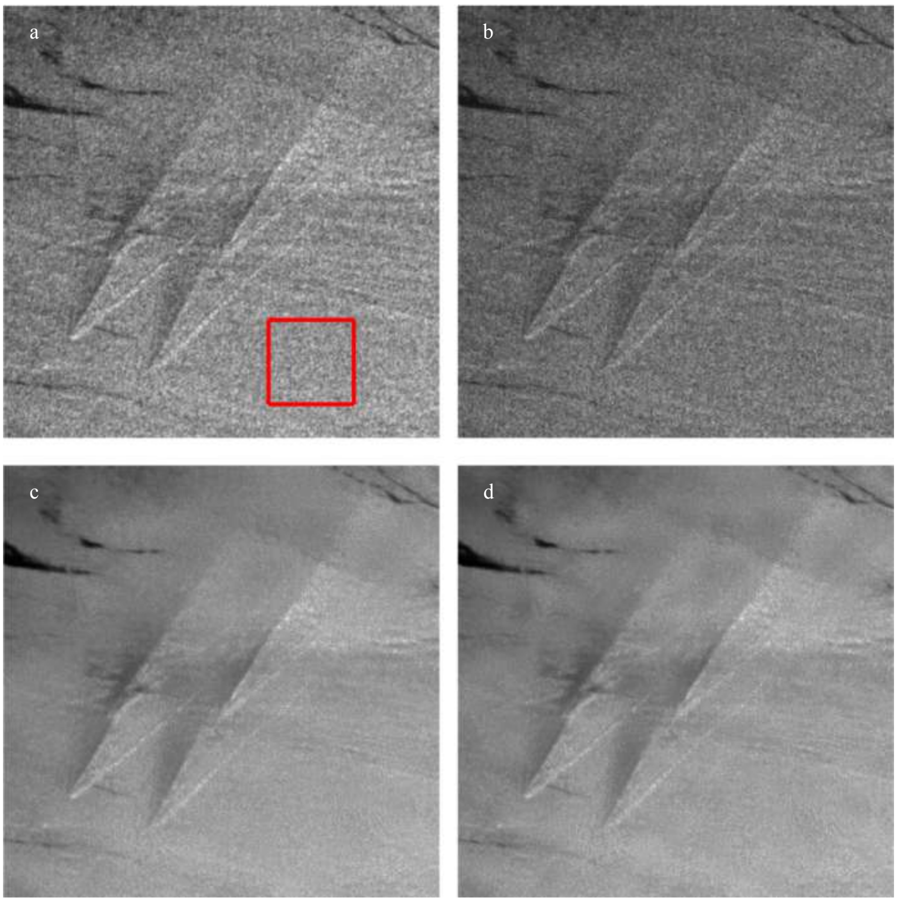

Fig. 3. Despeckled results for the image in Fig. 1a using the Lee filter (a), Frost filter (b), standard NLM algorithm (c), and proposed accelerated NLM algorithm (d). The red rectangle indicates the position of an approximately homogeneous region, which was used to calculate the STD and equivalent number of looks for the original noisy image and despeckled images, respectively.

Figures 3a–d show the despeckled results of Fig. 1a for visual inspection. Figure 3a shows the despeckled result of the Lee filter with a 3×3 window. It can be observed that speckle noise was suppressed to a certain extent. However, some block artifacts were introduced in homogeneous areas and some tiny details were smoothed. Figures 3b shows the despeckled results of the Frost filter with a 3×3 window. Speckle noise in homogenous areas was not suppressed effectively. The Frost filter also introduced blurring effects, but less intensely than the Lee filter. Figures 3c and d show the despeckled results of the standard NLM algorithm and the proposed accelerated NLM algorithm, respectively. We observe that both algorithms demonstrated good performance in terms of speckle reduction and detail preservation. Compared with the above two methods, speckle noise in the homogenous regions was efficiently removed. Furthermore, the despeckled result of the proposed speed-up NLM algorithm demonstrated good visual quality, but with higher computational efficiency.

Figures 4a–d provide the despeckled results of the Lee filter, Frost filter, standard NLM algorithm, and proposed fast NLM algorithm for the image in Fig. 1b. The Lee filter reduced speckle in homogeneous regions, but blurred fine edges and lines, and tended to introduce artifacts in homogenous regions. The Frost filter also blurred tiny details and thin lines, and the smoothness of homogeneous regions was not satisfying. The standard NLM algorithm not only smoothed homogenous regions, but also well preserved texture in the SAR image. The proposed improved NLM algorithm also effectively smoothed homogeneous regions while keeping textures, but with a lower computational cost.

For quantitative performance evaluations, the STD and equivalent number of looks (ENL) are calculated for original and processed images, respectively. The STD is given as

$$\sigma = \sqrt{\frac{1}{N}\sum_{i=1}^{N}(x_i - \mu)^2}, \tag{11}$$

where N is the image dimension, x_i is the gray value of Pixel i, and μ is the mean value of the image. Typically, a large STD corresponds to a higher noise level. The ENL is defined as

$$ENL = \frac{\mu^2}{\sigma^2}. \tag{12}$$

The ENL measures the degree of speckle reduction in a homogenous region. Typically, a higher ENL value corresponds to better speckle suppression. The value of the ENL typically depends on the size and location of the tested region. Theoretically, the tested region should be sufficiently large to provide a robust estimation of the ENL and meet the homogenous hypothesis in it.

As shown in Figs 3a and 4a, two approximately homogeneous regions were chosen and indicated by two red rectangles. The

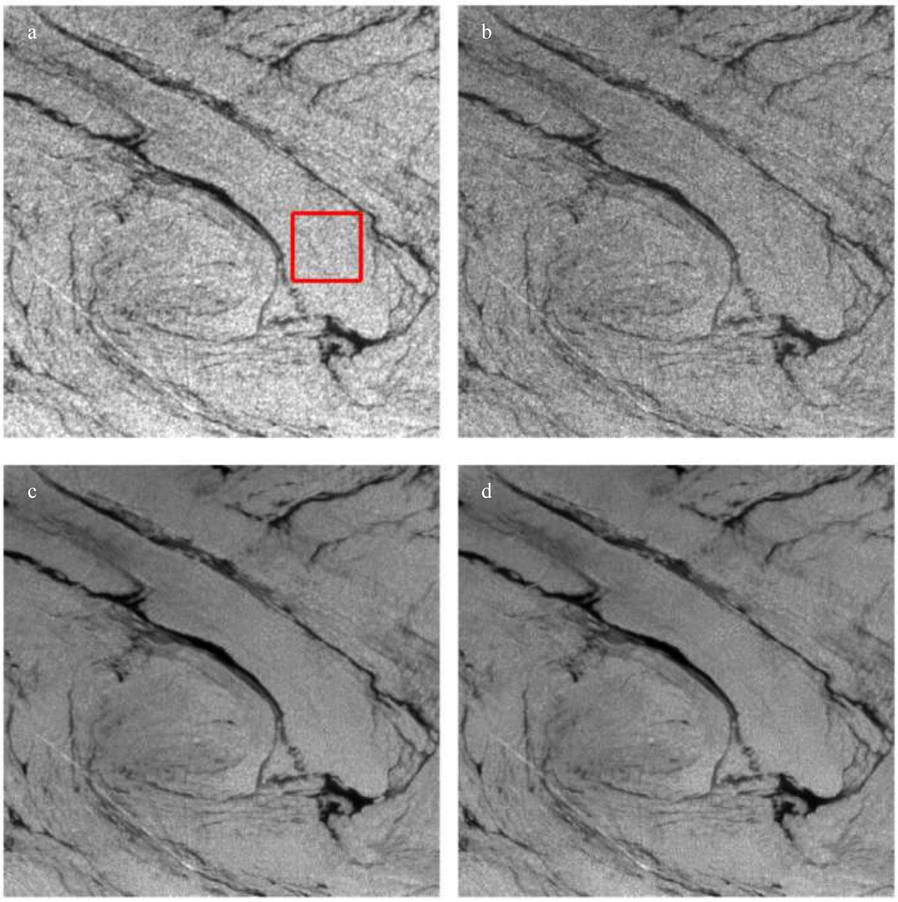

Fig. 4. Despeckled results of the image in Fig. 1b using the Lee filter (a), Frost filter (b), standard NLM algorithm (c), and proposed accelerated NLM algorithm (d). The red rectangle indicates the position of an approximately homogeneous region, which was used to calculate the STD and equivalent number of looks for the original noisy image and despeckled images, respectively.

STD and ENL for the two original noisy images and despeckled images, respectively, were calculated on these areas. The results are listed in Tables 1 and 2, respectively. We can see that the Lee and Frost filters also obtained better quantitative performance than the original noisy SAR images. The standard NLM algorithm presented the best results for the STD and ENL at the expense of increasing the computational complexity. The quantitative performance of the proposed fast NLM algorithm was also good, but slightly worse than the standard NLM algorithm. The reason for this is as follows: because the two parameters were calculated on flat regions, small similarity and search windows were used by the proposed NLM algorithm. However, the computational cost of the proposed algorithm greatly improved compared with the standard NLM algorithm. Considering the visual and quantitative assessments, we found that the method proposed in this paper had good despeckling ability. It not only suppressed speckle noise, but also preserved the fine details in SAR images.

Figures 5a and 6a show two noisy SAR ocean images, which demonstrate the signatures of oil films on the sea surface and an eddy, respectively. The two red rectangles indicate the positions of two approximately homogeneous regions. Figures 5b–d and 6b–d show the despeckled results of the Lee filter, Frost filter, and proposed fast NLM algorithm, respectively. As discussed above, the Lee and Frost filters did not sufficiently overcome the shortcomings of blurring texture and reducing speckle. The proposed algorithm simultaneously well preserved details and smoothed homogeneous areas. Tables 3 and 4 present the results of the STD and ENL. Finally, we found that the proposed NLM algorithm presented a good compromise between smoothing and edge preservation, with economic time cost.

Table 1. Quantitative measurements for Fig. 1a and the four despeckled images in Fig. 3

	Original image	Lee filter	Frost filter	Standard NLM	Accelerated NLM
STD	33.4	18.3	16.8	11.3	11.6
ENL	12.3	66.4	48.8	209.4	196.4

Table 2. Quantitative measurements for Fig. 1b and the four despeckled images in Fig. 4

	Original image	Lee filter	Frost filter	Standard NLM	Accelerated NLM
STD	42.8	23.2	22.1	15.2	15.8
ENL	12.1	63.4	45.6	91.4	84.9

Table 5 presents a comparison of the execution time between the proposed accelerated NLM algorithm and the standard NLM algorithm. The dimensions of Figs 3a, 4a, 5a and 6a are all 512×512. For each case, the proposed accelerated NLM algorithm and the standard NLM algorithm ran 100 and 5 times, respectively. The average execution time was calculated and is listed in Table 5. The unit of the execution time is seconds.

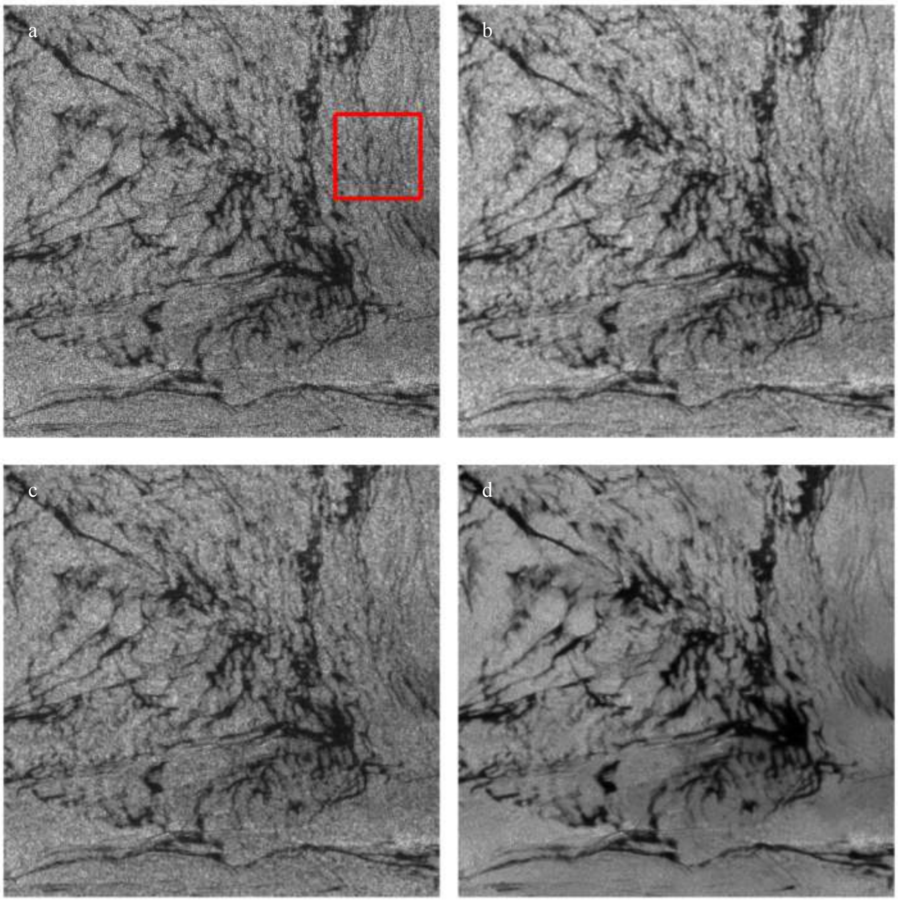

Fig. 5. Signatures of oil films on the sea surface. a. Original noisy SAR image; b. despeckled result of the Lee filter; c. despeckled result of the Frost filter; and d. despeckled result of the proposed accelerated NLM algorithm. The red rectangle indicates the position of an approximately homogeneous region.

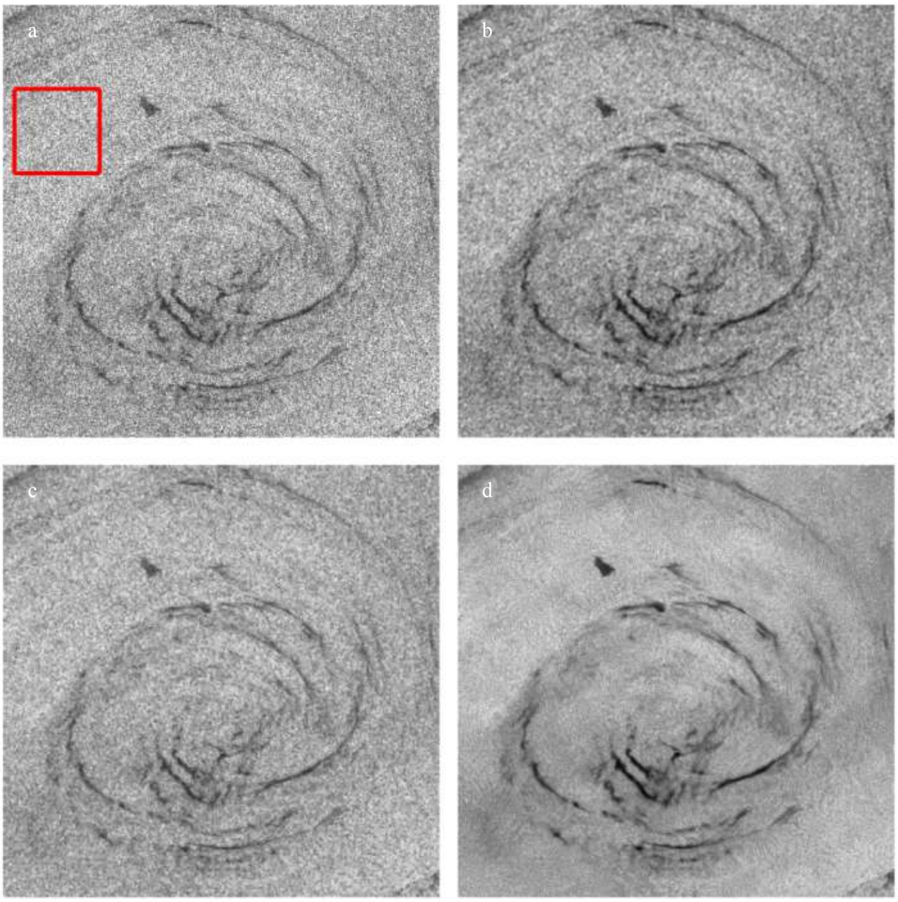

Fig. 6. Signatures of an eddy. a. Original noisy SAR image; b. despeckled result of the Lee filter; c. despeckled result of the Frost filter; and d. despeckled result of the proposed accelerated NLM algorithm. The red rectangle indicates the position of an approximately homogeneous region.

Table 3. Quantitative measurements for Fig. 5

	Original image	Lee filter	Frost filter	Standard NLM	Accelerated NLM
STD	38.3	26.3	24.4	18.6	18.7
ENL	8.8	23.9	21.8	34.7	34.6

Table 4. Quantitative measurements for Fig. 6

	Original image	Lee filter	Frost filter	Standard NLM	Accelerated NLM
STD	46.7	21.8	23.8	19.4	20.1
ENL	17.4	61.1	57.4	91.3	84.4

Table 5. Execution time of the proposed accelerated NLM algorithm and the standard NLM algorithm

	Fig. 3a	Fig. 4a	Fig. 5a	Fig. 6a
Execution time ofstandard NLM algorithms/s	16.077	16.077	16.077	16.077
Execution time ofproposed NLM algorithms/s	0.076	0.081	0.083	0.078

6 Discussion and conclusions

SAR images are widely used in various fields of ocean science and engineering. This paper is mainly concerned with speckle suppression in applications such as automatic target detection, classification, and tracking. We attempted to improve the readability of SAR images for detecting objects and regions of interest. SAR images are also a popular tool for the retrieval of sea surface wind fields and waves. We are uncertain about the impact of the NLM despeckling on these applications. By exploiting image self-similarity, the NLM algorithm removes speckle noise by building statistical averaging of pixels that have similar textural structures for image patches. It is not clear whether the useful information for the retrieval of sea surface wind fields and waves may be distorted during filtering operations. Furthermore, what feature or feature vector is selected to measure the similarity between image patches is an important issue. More studies on this issue need to be conducted on in future work.

A rapid NLM algorithm for SAR ocean images despeckling is introduced in this paper. Each pixel does not exist in isolation but constitutes a textural structure with surrounding pixels in a SAR image. For each pixel, a local window is chosen with the pixel as the center. The pixel is considered as a flat pixel if the gray values vary smoothly among pixels in the window; otherwise, it is considered as a texture pixel. Mathematically, gray gradients are calculated along four directions. If the maximum gray gradient is larger than a predetermined threshold, then the pixel is considered as a texture pixel; otherwise, it is considered as a flat pixel. The above calculations are independent for each pixel. Thus, the indices of texture and flat pixels are obtained. According to the indices, different sizes of similarity and search windows are used on texture and flat pixels during NLM despeckling, respectively. Furthermore, the calculations consumed in calculating the Euclidean distances between patches and the normalizing factors are independent. The computational complexity of the developed NLM algorithm is reduced by introducing a CUDA-based GPU implementation of the algorithm. The proposed NLM despeckling algorithm presents a good compromise between smoothing and edge preservation with economic computational cost. Experiments demonstrated that computational efficiency improved by approximately 200 times over a plain CPU implementation of the standard NLM algorithm.

Acknowledgements

We thank the scientists involved in the Dragon Program.

References

Achim A, Tsakalides P, Bezerianos A. 2003. SAR image denoising via Bayesian wavelet shrinkage based on heavy-tailed modeling. IEEE Transactions on Geoscience and Remote Sensing, 41(8): 1773–1784, doi: 10.1109/TGRS.2003.813488

Alpers W, Brandt P, Lazar A, et al. 2013. A small-scale oceanic eddy off the coast of west Africa studied by multi-sensor satellite and surface drifter data. Remote Sensing of Environment, 129: 132–143, doi: 10.1016/j.rse.2012.10.032

Argenti F, Alparone L. 2002. Speckle removal from SAR images in the undecimated wavelet domain. IEEE Transactions on Geoscience and Remote Sensing, 40(11): 2363–2374, doi: 10.1109/TGRS.2002.805083

Aubert G, Aujol J F. 2008. A variational approach to removing multiplicative noise. SIAM Journal on Applied Mathematics, 68(4): 925–946, doi: 10.1137/060671814

Bilcu R C, Vehvilainen M. 2007. Fast nonlocal means for image denoising. In: Proceedings of SPIE 6502, Digital Photography III. San Jose, CA, USA: SPIE, doi: 10.1117/12.695079

Buades A, Coll B, Morel J M. 2005. A review of image denoising algorithms, with a new one. Multiscale Modeling & Simulation, 4(2): 490–530

Cuomo S, de Michele P, Piccialli F. 2014. 3D Data denoising via nonlocal means filter by using parallel GPU strategies. Computational and Mathematical Methods in Medicine, 2014: 523862, doi: 10.1155/2014/523862

Dabov K, Foi A, Katkovnik V, et al. 2007. Image denoising by sparse 3-D transform-domain collaborative filtering. IEEE Transactions on Image Processing, 16(8): 2080–2095, doi: 10.1109/TIP.2007.901238

Deledalle C A, Duval V, Salmon J. 2012. Non-local methods with shape-adaptive patches (NLM-SAP). Journal of Mathematical Imaging and Vision, 43(2): 103–120, doi: 10.1007/s10851-011-0294-y

Feng Chaolu, Zhao Dazhe, Huang Min. 2016. Image segmentation using CUDA accelerated non-local means denoising and bias correction embedded fuzzy c-means (BCEFCM). Signal Processing, 122: 164–189, doi: 10.1016/j.sigpro.2015.12.007

Foucher S, Farage G, Benie G. 2006. SAR image filtering based on the stationary contourlet transform. In: Proceeding of 2006 IEEE International Symposium on Geoscience and Remote Sensing. Denver, Colorado, USA: IEEE, 4021–4024

Frost V S, Stiles J A, Shanmugan K S, et al. 1982. A model for radar images and its application to adaptive digital filtering of multiplicative noise. IEEE Transactions on Pattern Analysis and Machine Intelligence, PAMI-4(2): 157-166

Goossens B, Luong H, Aelterman J, et al. 2010. A GPU-accelerated real-time NLMeans algorithm for denoising color video sequences. In: Proceedings of the 12th International Conference on Advanced Concepts for Intelligent Vision Systems. Sydney, Australia: Springer, 46–57, doi: 10.1007/978-3-642-17691-3_5

Johannessen J A, Shuchman R A, Digranes G, et al. 1996. Coastal ocean fronts and eddies imaged with ERS 1 synthetic aperture radar. Journal of Geophysical Research, 101(C3): 6651–6667, doi: 10.1029/95JC02962

Katkovnik V, Foi A, Egiazarian K, Astola J. 2010. From local kernel to nonlocal multiple-model image denoising. International Journal of Computer Vision, 86(1): 1–32, doi: 10.1007/s11263-009-0272-7

Kervrann C, Boulanger J, Coupé P. 2007. Bayesian non-local means filter, image redundancy and adaptive dictionaries for noise removal. In: Proceeding of the 1st International Conference on Scale Space and Variational Methods in Computer Vision. Ischia, Italy: Springer, 4485: 520-532

Kuan D, Sawchuk A, Strand T, et al. 1987. Adaptive restoration of images with speckle. IEEE Transactions on Acoustics, Speech, and Signal Processing, 35(3): 373–383, doi: 10.1109/TASSP.1987.1165131

Lee J S. 1980. Digital image enhancement and noise filtering by use of local statistics. IEEE Transactions on Pattern Analysis and Machine Intelligence, PAMI-2(2): 165–168

Li Ying, Gong Hongli, Feng Dagan, et al. 2011. An adaptive method of speckle reduction and feature enhancement for SAR images based on curvelet transform and particle swarm optimization. IEEE Transactions on Geoscience and Remote Sensing, 49(8): 3105–3116, doi: 10.1109/TGRS.2011.2121072

Li Xiaoming, Lehner S, Bruns T. 2014. Simultaneous measurements by advanced SAR and radar altimeter on potential improvement of ocean wave model assimilation. IEEE Transactions on Geoscience and Remote Sensing, 52(5): 2508–2518, doi: 10.1109/TGRS.2013.2262137

Liu A K, Chang Y S, Hsu M K, et al. 1998. Evolution of nonlinear internal waves in the East and South China Sea. Journal of Geophysical Research, 103(C4): 7995–8008, doi: 10.1029/97JC01918

Lopes A, Touz R, Nezry E. 1990. Adaptive speckle filters and scene heterogeneity. IEEE Transactions on Geoscience and Remote Sensing, 28(6): 992–1000, doi: 10.1109/36.62623

Márques A, Pardo A. 2013. Implementation of non local means filter in GPUs. In: Proceedings of the 18th Iberoamerican Congress Progress in Pattern Recognition, Image Analysis, Computer Vision, and Applications. Havana, Cuba: Springer, 407–414, doi: 10.1007/978-3-642-41822-8_51

Parrilli S, Poderico M, Angelino C V, et al. 2012. A nonlocal SAR image denoising algorithm based on LLMMSE wavelet shrinkage. IEEE Transactions on Geoscience and Remote Sensing, 50(2): 606–616, doi: 10.1109/TGRS.2011.2161586

Shen Hui, Perrie W, Liu Qingrong, et al. 2014. Detection of macroalgae blooms by complex SAR imagery. Marine Pollution Bulletin, 78(1–2): 190–195, doi: 10.1016/j.marpolbul.2013.10.044

Solberg A H S, Brekke C, Husoy P O. 2007. Oil spill detection in Radarsat and Envisat SAR images. IEEE Transactions on Geoscience and Remote Sensing, 45(3): 746–755, doi: 10.1109/TGRS.2006.887019

Vignesh R, Tae Oh B, Jay Kuo C C. 2010. Fast non-local means (NLM) computation with probabilistic early termination. IEEE Signal Processing Letters, 17(3): 277–280, doi: 10.1109/LSP.2009.2038956

Walessa M, Datcu M. 2000. Model-based despeckling and information extraction from SAR images. IEEE Transactions on Geoscience and Remote Sensing, 38(5): 2258–2269, doi: 10.1109/36.868883

Wang Jin, Guo Yanwen, Ying Yiting, et al. 2006. Fast non-local algorithm for image denoising. In: Proceedings of 2006 IEEE International Conference on Image Processing. Atlanta, GA, USA: IEEE, 1429–1432, doi: 10.1109/ICIP.2006.312698

Wang Juan, Huang Weigen, Yang Jingsong, et al. 2013. Study of the propagation direction of the internal waves in the South China Sea using satellite images. Acta Oceanologica Sinica, 32(5): 42–50, doi: 10.1007/s13131-013-0312-6

Wu Yifeng, Maitre H. 1992. Smoothing speckled synthetic aperture radar images by using maximum homogeneous region filters. Optical Engineering, 31(8): 1785–1792, doi: 10.1117/12.59897

Xie Hua, Pierce L E, Ulaby F T. 2002. SAR speckle reduction using wavelet denoising and Markov random field modeling. IEEE Transactions on Geoscience and Remote Sensing, 40(10): 2196–2212, doi: 10.1109/TGRS.2002.802473

Xue Bindang, Huang Yuan, Yang Jihong, et al. 2013. Fast nonlocal remote sensing image denoising using cosine integral images. IEEE Geoscience and Remote Sensing Letters, 10(6): 1309–1313, doi: 10.1109/LGRS.2013.2238603

Yang Jungang, Zhang Jie, Meng Junmin. 2010. A detection model of underwater topography with a series of SAR images acquired at different time. Acta Oceanologica Sinica, 29(4): 28–37, doi: 10.1007/s13131-010-0048-5

Zheng Quanan, Susanto R D, Ho C R, et al. 2007. Statistical and dynamical analyses of generation mechanisms of solitary internal waves in the northern South China Sea. Journal of Geophysical Research, 112(C3): C03021, doi: 10.1029/2006JC003551

Zhong Hua, Zhang Jingjing, Liu Ganchao. 2014. Robust polarimetric SAR despeckling based on nonlocal means and distributed Lee filter. IEEE Transactions on Geoscience and Remote Sensing, 52(7): 4198–4210, doi: 10.1109/TGRS.2013.2280278